Detection of Biolayer Formation Instant in SPR Biosensors Using Neural Networks

Rafael Pereira do Nascimento
Department of Electrical Engineering
Federal University of Paraíba
João Pessoa, Paraíba, Brazil
rafaelp.nascimento@estudante.cear.ufpb.br

Carlos Alberto de Souza Filho
Department of Electrical Engineering
Federal University of Paraíba
João Pessoa, Paraíba, Brazil
calberto@cear.ufpb.br

Antônio Marcus Nogueira Lima
Department of Electrical Engineering
Federal University of Campina Grande
Campina Grande, Paraíba, Brazil
amnlima@ee.ufcg.edu.br

ABSTRACT

This work presents a method for detecting the biolayer formation instant in surface plasmon resonance (SPR) biosensors using signal processing and artificial intelligence. The proposed approach combines the wavelet transform (WT) with a multi-layer perceptron (MLP) neural network to analyze the asymmetry in the SPR response. Experimental data were collected from BSA adsorption cycles using an SPR biosensor and the VIR biochip. After preprocessing and feature extraction using the Daubechies db4 wavelet, the MLP was trained to recognize the characteristic pattern associated with monolayer formation. The model achieved over 99% accuracy, with an average temporal error of less than 3 seconds. The technique enables early detection of the biolayer formation, reducing reagent consumption and shortening the experimental duration by up to 474 seconds per cycle. These results demonstrate the potential of the method for automating functionalization steps in SPR-based biosensors, especially in cost-sensitive applications.

KEYWORDS: SPR biosensor, biolayer detection, wavelet transform, neural network, BSA adsorption, signal processing

1 Introduction

Surface plasmon resonance (SPR) spectroscopy is a well-established optical technique, particularly employed for the detection of biochemical events without the need for fluorescent or radioactive labels [5].

SPR-based biosensors stand out due to their high sensitivity, ability to monitor kinetic biomolecular interactions in real-time, resistance to electromagnetic interference, and label-free operation. They are widely used in biomedical research and clinical diagnostics [1, 6, 12, 21], food safety [2, 11, 20], and environmental monitoring [8, 10, 14]. With a specific biomolecular recognition layer and appropriate surface preparation techniques, these sensors are capable of accurately detecting targets such as viruses, bacteria, antibodies, and other biomarkers [12].

Despite the potential of SPR biosensors to monitor molecular interactions in real-time, their application presents technical and analytical challenges. One of the main obstacles lies in the formation of biochemical layers on the sensor surface, a process that can require a significant amount of material and result in considerable waste during the adsorption process. As part of the preparation protocol, the surface must be rinsed with water to remove weakly bound compounds and ensure the formation of a stable monolayer. However, this step leads to material waste, particularly when researchers use expensive and specific compounds in the sensitive layer. The price of these materials can reach up to USD 5,900.00 per milligram [3], making process optimization essential to minimize waste and reduce operational costs.

The evaluation of the quality of biochemical layers involves various characterization methods that allow the investigation of their structural, chemical, and functional properties. Among the available techniques are X-ray photoelectron spectroscopy (XPS) [15], atomic force microscopy (AFM) [7], spectroscopic ellipsometry [16], Fourier-transform infrared spectroscopy (FTIR) [13], electrochemical impedance spectroscopy (EIS) [4, 18], and cyclic voltammetry [18].

Although there are several techniques for evaluating the characteristics that determine the quality of the layer, the methods mentioned perform analyses comparing the results before and after the layer formation process. Therefore, these techniques cannot determine when the sensor forms new layers during the sequential passage of substances.

Artificial intelligence (AI) techniques have been used to optimize sensor construction parameters, reduce measurement error, improve sensitivity in disease detection [5, 20], improve data analysis, reduce noise, and enable predictive modeling [6].

Although significant progress has been reported in the literature regarding the formation of the sensitive layer, the absence of reliable methods for determining the precise moment of biolayer formation on the surface of SPR biosensors remains an unresolved challenge.

This article proposes a technique for detecting and analyzing the biolayer formation process in SPR biosensors, which allows for the identification of changes occurring on the sensor surface during the experiment, identifying the instant of layer formation without the need to wait for the biosensor output signal to stabilize. The proposed method utilizes artificial neural networks to detect the instant of layer formation by monitoring variations in the refractive index and the asymmetry of the SPR curve.

2 Curve Morphology

Changes in the substance analyzed by the biosensor modify the resonance condition, causing a shift in the SPR curve, as shown in Fig. 1(a). The resonance angle θ_R depends on the refractive index and the thickness of the sensitive layer. From θ_R, one can determine the effective refractive index of the solution, n_{eff}. In biosensors using angular interrogation mode, the sensorgram is obtained by monitoring over time the value of θ_R, n_{eff}, or the variation relative to the refractive index of water (Δn_{eff}).

Changes in the analyzed solution also affect the shape of the SPR curve. Thus, analyzing the curve morphology over time can be used to monitor specific characteristics of the substance under study. The inset graphs in Fig. 1 show that variations in the refractive index of the samples can be identified through changes in both the resonance angle θ_R and the curve asymmetry G

The analysis of SPR curve morphology relies on observing parameters such as the full width at half maximum (Γ) and the asymmetry (G), as illustrated in Fig. 1.

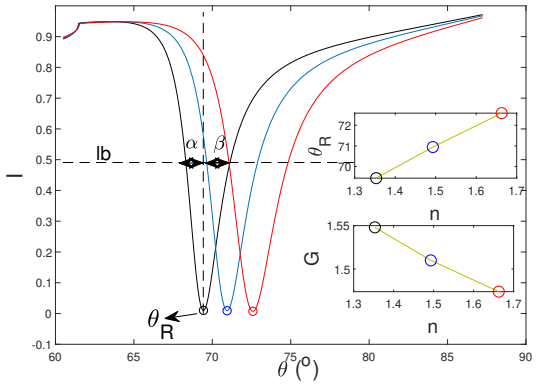

Figure 1. SPR curve morphology characteristics.

The curve width Γ is calculated at the full width at half maximum (FWHM) of the SPR curve. Initially, the mean intensity value (lb) represented by the line in Fig. 1 is determined. This value is obtained by averaging the maximum and minimum points of the SPR curve. The value of Γ is then obtained from the distance between the left and right edges of the curve. To determine the minimum of the curve, techniques such as the first moment method and polynomial fitting are used to identify the resonance condition.

To determine the asymmetry G, the resonance angle θ_R must first be found. Then, the distances from the minimum point to the left edge (α) and to the right edge (β) of the SPR curve are calculated, both at the mean intensity level (lb). The asymmetry value is defined as the ratio between the two halves of the curve relative to the minimum point and can be calculated by (1).

$$G = \frac{\beta}{\alpha} \tag{1}$$

Here, G represents the difference in size between the right edge and the left edge.

3 Proposed Technique

The adsorption process of bovine serum albumin (BSA) on gold surfaces is frequently described as an exothermic phenomenon in which the interaction between protein molecules and the metallic surface results in energy release [9].

In [15] it was shown that Γ e G can be represented as a function of four independent contributions, among which a portion is strongly dependent on the temperature variation. The authors identified that the peaks in the asymmetry signal coincide with the time of layer formation, which can be explained by the increase in temperature caused by the exothermic reaction. The adsorption process of biomolecules can lead to exothermic or endothermic reactions, which cause temperature variations in the sensitive layer, causing changes mainly in the G value.

This work proposes the use of the asymmetry signal to monitor changes associated with the adsorption process of molecules and, consequently, with the formation of the biolayer in SPR biosensors. The proposed technique allows the identification of the moment of layer formation, which can be divided into four steps:

1. Acquisition of θ_R and G;
2. Preprocessing of the data;
3. Calculation of the wavelet transform of the asymmetry signal;
4. Normalization and application of the neural network.

3.1 Layer Formation Instant

In the standard procedure for layer formation, after introducing the substance into the biosensor, one must wait for the stabilization of the effective refractive index before proceeding with the next substance. This moment is indicated by time t_e, as shown in Fig. 2. The stabilization of Δn_{eff} indicates that no further changes are occurring in the formed layer. After this point, water is introduced to remove reversibly bound molecules held by weak interactions.

The proposed solution aims to identify the instant of formation (t_{ref} in Fig. 2) of the BSA layer within region "A", where the refractive index reaches the same value observed after the removal of weakly bound molecules in the region "B". This point is highlighted in Fig. 2 with a blue extension indicating the corresponding refractive index value. This approach enables the identification of layer formation in the region "A" without the need to wait for complete refractive index stabilization, thereby reducing experiment time and saving material.

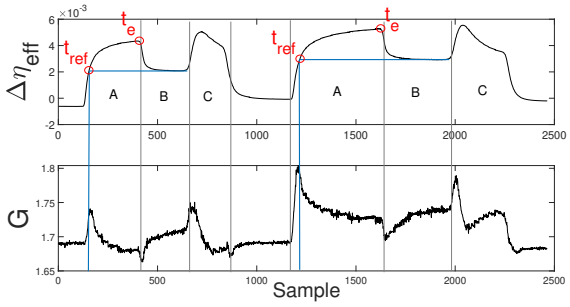

Figure 2. BSA adsorption cycle using polynomial fitting: variation of refractive index and asymmetry

3.2 Acquisition of θ_R and G

The resonance angle θ_R is obtained using two different techniques: polynomial fitting and the first moment method. The value of G is calculated as described in section 2. Based on the value of θ_R, the effective refractive index n_{eff} is computed using the three-layer Fresnel model [19].

3.3 Data Preprocessing

Signal preprocessing was performed in MATLAB to enhance data quality for subsequent analysis. The time series of the SPR curve asymmetry and the variation in effective refractive index were processed using a median filter followed by three iterations of a moving average filter, both of which were applied with a sliding window of 15 samples.

3.4 Wavelet Transform of the Asymmetry Signal

To highlight the variations associated with biolayer formation, the wavelet transform was applied to the asymmetry signal. The Daubechies wavelet of order 4 (db4) was selected for its sensitivity to short-duration transients and its balanced trade-off between temporal and spectral resolution. This characteristic is essential for detecting subtle patterns associated with the adsorption process. Additionally, the db4 wavelet offers strong noise robustness, enabling efficient and accurate signal decomposition.

3.5 Normalization and NN Application

After applying the wavelet transform, the fourth detail level was found to provide the most representative pattern for identifying the instant of layer formation. This pattern is characterized by oscillations that begin with the introduction of BSA, intensify until reaching a peak, and then decay, indicating system stabilization.

The interval between the onset of oscillations and the peak defines a temporal signature representing the formation of the biolayer (Fig. 3(c) and Fig. 3(d)). This pattern was used to configure the output variables of the neural network, enabling automatic recognition of this behavior in the input data.

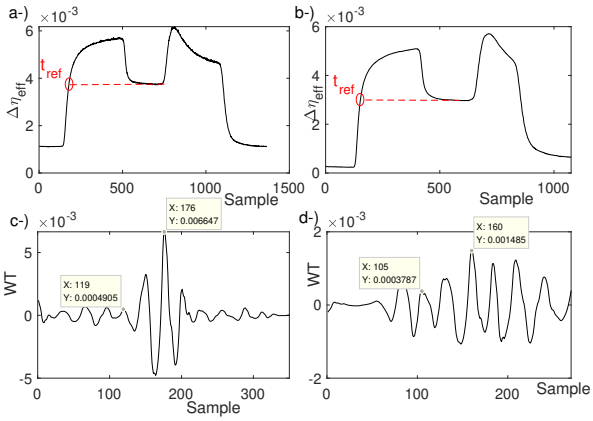

Figure 3. Oscillatory pattern used to identify the instant of biolayer formation. Top graphs: variation in refractive index; bottom: wavelet coefficients (level 4). Left: first moment method; right: polynomial fitting.

The proposed methodology relies on detecting a specific pattern in the level-4 wavelet transform (WT). The presence of this signature in the signal is interpreted as an indication of the adsorption process.

To enable supervised training of the neural network, the data were normalized using the min-max method and labeled according to the presence or absence of the characteristic pattern. Windows containing the pattern were labeled as class 1; otherwise, they were labeled as class 0. A total of 1,063 positive and 20,862 negative samples were identified, considering signals processed using both the first moment and polynomial fitting methods.

The MLP model was implemented in Python using the TensorFlow and scikit-learn libraries. The dataset was split into 80% for training and 20% for testing, with early stopping employed to prevent overfitting. Optimization was performed using the Adam algorithm and the binary cross-entropy loss function.

The neural network consists of two hidden layers, each with 64 and 32 neurons, respectively, both of which are activated by ReLU functions. The output layer has a single neuron with a sigmoid activation function (Fig. 4(a)). The network input is formed by a sliding window of size 100, containing the values of the variation in effective refractive index and the wavelet transform of the asymmetry signal, including the current value and the previous 100 values for each variable.

4 Results and Analysis

To evaluate the effectiveness of the proposed technique, seven experimental adsorption cycles of the BSA molecule were carried out using the SPR biosensor developed by [17], based on the VIR biochip proposed by [19].

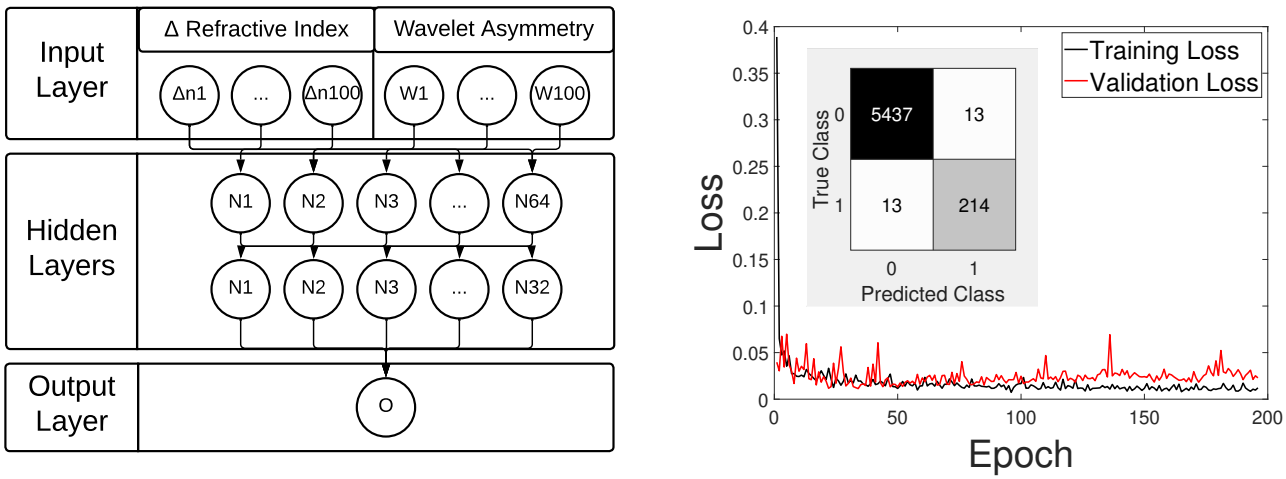

(a) Neural network architecture

(b) Network performance

Figure 4. Neural network architecture and performance evaluation.

The adsorption cycle illustrated in Fig. 2 is divided into five stages. Initially, degassed and deionized water is introduced into the system to stabilize the equipment. Then, in region "A", a 1% aqueous solution of BSA is injected, during which the first layer begins to form through the binding of the protein to the gold surface. After this step, the system is left to stabilize until the refractive index reaches a steady-state regime. In region "B", the surface is rinsed with water to remove the weak, reversible BSA bonds. Immediately after, in region "C", a 10% sodium hypochlorite solution is introduced to eliminate the adsorbed BSA layer by breaking the strong (irreversible) bonds with the gold. Finally, a new water rinse is performed to remove the hypochlorite and restore the system's initial conditions.

A total of 21,925 samples were collected, with an acquisition frequency of 1.25 Hz (sampling interval of 0.8 seconds).

4.1 Normalization and NN Application

During training, the model achieved stable convergence in approximately 200 epochs, thanks to the use of the early stopping strategy with a patience of 100 epochs. This approach ensured that training stopped at the optimal point, preventing overfitting and promoting good generalization capability.

Fig. 4(b) shows the neural network's performance. The loss curve indicates that training (black) and validation (red) losses remained close throughout the epochs, suggesting stable convergence and the absence of overfitting. Furthermore, the embedded confusion matrix reveals 5,865 correct classifications and 26 errors, with an equal distribution between false positives and false negatives. These results demonstrate the model's high accuracy and strong generalization.

The MLP performance metrics are presented in Table 1. Both techniques (first moment and polynomial fitting) achieved accuracy above 99%, with F1-scores close to 1, confirming the model's effectiveness in detecting the instant of layer formation.

Table 1. Performance comparison of the neural network using first moment and polynomial fitting data.

Metric	First Moment	Polynomial Fitting
Accuracy	99.45%	99.31%
Sensitivity	92.26%	92.75%
Specificity	99.89%	93.09%
F1-Score	0.9509	0.9993

Fig. 5 shows the results from the neural network trained with data processed via polynomial fitting for seven adsorption cycles. The first three plots display the variation in refractive index, asymmetry, and wavelet transform, respectively. The red-shaded area indicates the interval in which the network recognized the biolayer formation pattern. The fourth plot presents the post-processed network output, highlighting the detected instant of layer formation. To reduce false positives, a criterion was applied that only considers transitions from 0 to 1 if followed by at least two consecutive high-level samples. The black signal indicates the network-detected point, while the red signal represents the reference value. The close alignment of both signals demonstrates the model's accuracy.

Two distinct peaks are observed, resulting from a brief failure in pattern detection that was quickly corrected, demonstrating the model's resilience to minor signal variations. Similar results were observed with the first moment technique.

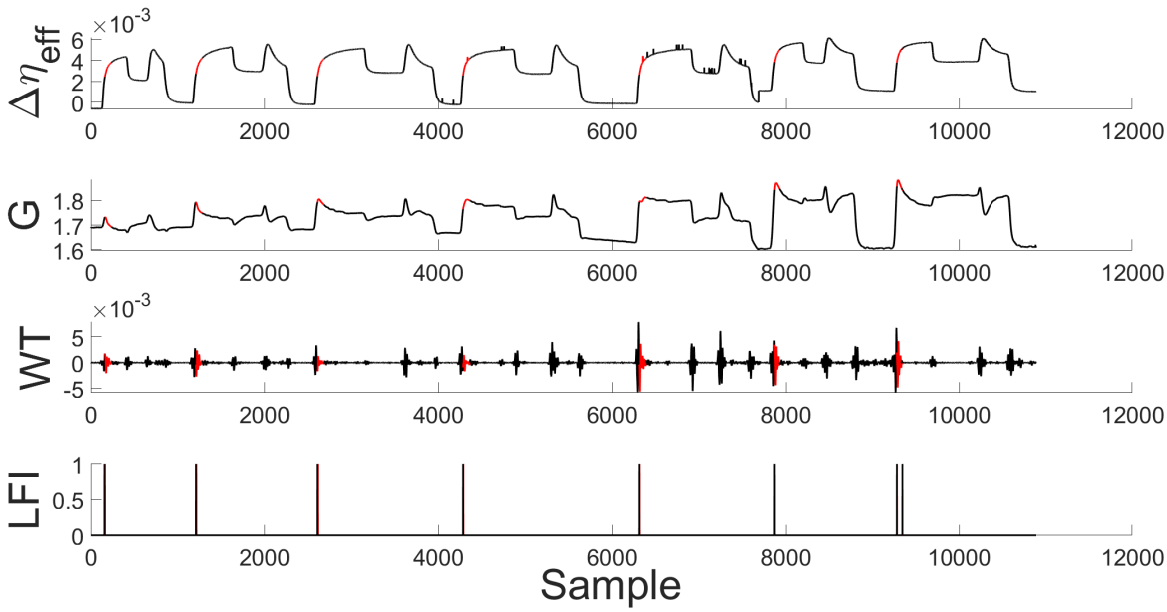

Figure 5. Neural network results using polynomial fitting.

To further assess performance, the error (e) between the instant identified by the network (t_r) and the reference instant (t_{ref}), corresponding to the time just before reversible binding, was calculated. Table 2 presents the results for both the first moment method (index 1) and polynomial fitting (index p) across seven experimental cycles.

To compare the proposed technique with the traditional method based on refractive index stabilization, the time savings were estimated. The saved time E was calculated as the difference between the stabilization time (t_e), shown in Fig. 2, and the time predicted by the network (t_r), according to $E = t_e - t_r$. The data are summarized in Table 2.

The results show a significant reduction in experiment time using both approaches, with up to 474.4 seconds achieved with the first moment method and 472 seconds with polynomial fitting. In both cases, the neural network accurately described the signal behavior and adapted efficiently to variations across the cycles.

In practice, this reduction results from a shorter exposure time to the reagent. Since the model anticipates monolayer formation, the flow of the active substance can be stopped earlier, thereby reducing material consumption, a particularly important factor in applications involving costly reagents.

5 Conclusion

The methodology developed in this study proved highly effective for the automatic detection of biolayer formation in SPR-based biosensors. The combination of wavelet transform, used to enhance transients in the asymmetry signal, with a multilayer perceptron (MLP) neural network enabled precise identification of the characteristic adsorption pattern of BSA on the sensor surface.

The results obtained from seven experimental cycles demonstrated robust model performance, with accuracy exceeding 99%, sensitivity above 92%, and an average error of less than 3 seconds relative to the reference point defined by refractive index stabilization. The proposed approach yielded consistent results using both the first moment method and polynomial fitting.

Beyond its precision, the technique demonstrated significant time savings in the experiment. Anticipating the instant of biolayer formation reduced the total adsorption time per cycle by up to 474 seconds. This reduction directly impacts reagent consumption, which is particularly advantageous in experiments involving costly or limited-availability substances.

From a practical standpoint, the proposed technique can significantly contribute to automating SPR biosensor processes by enabling real-time control strategies for functionalization stages involving automatic substance exchanges. Its application can facilitate the development of more efficient, accurate, and cost-effective systems, expanding the use of biosensors in both laboratory and industrial settings.

Future work includes applying the methodology to other types of biomolecules and functionalized surfaces, as well as validating the model across different SPR platforms. Moreover, exploring more advanced neural network architectures is a promising way to improve detection accuracy and robustness.

Table 2. Performance evaluation

No.	t_{e1}	e_1	E_1	t_{ep}	e_p	E_p
1	399	7 (5.6 s)	240 (192 s)	407	6 (4.8 s)	246 (196.8 s)
2	1627	0 (0 s)	418 (334.4 s)	1625	-5 (-4 s)	409 (327.2 s)
3	3128	0 (0 s)	522 (417.6 s)	3143	-7 (-5.6 s)	530 (424 s)
4	4860	1 (0.8 s)	573 (458.4 s)	4868	-3 (-2.4 s)	580 (464 s)
5	6906	2 (1.6 s)	593 (474.4 s)	6906	-3 (-2.4 s)	590 (472 s)
6	8328	1 (0.8 s)	314 (251.2 s)	8191	1 (0.8 s)	321 (256.8 s)
7	9820	-1 (-0.8 s)	395 (316 s)	9676	-1 (-0.8 s)	395 (316 s)

ACKNOWLEDGMENTS

This work has been funded by the project 'SMARTSENS Base System' supported by CENTRO DE COMPETÊNCIA EMBRAPII VIRTUS EM HARDWARE INTELIGENTE PARA INDÚSTRIA - VIRTUS-CC, with financial resources from the PPI HardwareBR of the MCTI grant number 055/2023, signed with EMBRAPII.

REFERENCES

[1] Na An, Kai Li, Yukun Zhang, Tingting Wen, Weixiao Liu, Gang Liu, Liang Li, and Wujun Jin. 2021. A multiplex and regenerable surface plasmon resonance (MR-SPR) biosensor for DNA detection of genetically modified organisms. *Talanta* 231 (2021), 122361. doi:10.1016/J.TALANTA.2021.122361

[2] Md Tauseef Iqbal Ansari, Sanjeev Kumar Raghuwanshi, and Santosh Kumar. 2023. Recent Advancement in Fiber-Optic-Based SPR Biosensor for Food Adulteration Detection—A Review. *IEEE Transactions on NanoBioscience* 22, 4 (2023), 978–988. doi:10.1109/TNB.2023.3278468

[3] Antibodies. 2023. *Price Comparison - Antibodies.* Retrieved Oct 09, 2024 from https://www.antibodies.com/price-comparison

[4] Shaojun Dong and Jinghong Li. 1997. Self-assembled monolayers of thiols on gold electrodes for bioelectrochemistry and biosensors. *Bioelectrochemistry and Bioenergetics* 42, 1 (1997), 7–13. doi:10.1016/S0302-4598(96)05172-0

[5] Jiri Homola, Susan S. Yee, and Gunther Gauglitz. 1999. Surface plasmon resonance sensors: review. *Sensors and Actuators B: Chemical* 54, 1-2 (1999), 3–15.

[6] Rajeev Kumar, Lokendra Singh, and S. Malathi. 2025. Infected and Noninfected Diseases Detection for Human Health Using Surface Plasmon Resonance Biosensors: A Review. *IEEE Sensors Journal* 25, 7 (2025), 10556–10565. doi:10.1109/JSEN.2025.3539783

[7] Jung Wook Lee, Sang Jun Sim, Sung Min Cho, and Jeewon Lee. 2005. Characterization of a self-assembled monolayer of thiol on a gold surface and the fabrication of a biosensor chip based on surface plasmon resonance for detecting anti-GAD antibody. *Biosensors and Bioelectronics* 20 (2005), 1422–1427. doi:10.1016/j.bios.2004.04.017

[8] Mansour Mahmoudpour, Jafar Ezzati Nazhad Dolatabadi, Mohammadali Torbati, and Aziz Homayouni-Rad. 2019. Nanomaterials based surface plasmon resonance signal enhancement for detection of environmental pollutions. *Biosensors and Bioelectronics* 127 (2019), 72–84.

[9] M.S. Maleki, O. Moradi, and S. Tahmasebi. 2017. Adsorption of albumin by gold nanoparticles: Equilibrium and thermodynamics studies. *Arabian Journal of Chemistry* 10 (2017), S491–S502. doi:10.1016/j.arabjc.2012.10.009

[10] Xiaojian Meng, Xiaokang Wang, Kun Yu, Yufang Liu, and Shuguang Li. 2025. Lab on Fiber: Recent Experimental Advances in Optical Fiber Sensor Based on Surface Plasmon Resonance. *IEEE Transactions on Instrumentation and Measurement* 74 (2025), 1–19. doi:10.1109/TIM.2025.3547521

[11] Md Moznuzzaman, Md Rafiqul Islam, Md Biplob Hossain, and Ibrahim Mustafa Mehedi. 2020. Modeling of highly improved SPR sensor for formalin detection. *Results in Physics* 16 (2020), 102874.

[12] Sharifah Norsyahindah Syed Nor, Nur Syafiqah Rasanang, Salmah Karman, Wan Safwani Wan Kamarul Zaman, Sulaiman Wadi Harun, and Hamzah Arof. 2021. A review: surface plasmon resonance-based biosensor for early screening of SARS-CoV2 infection. *IEEE Access* 10 (2021), 1228–1244.

[13] R. M. Nyquist, A. S. Eberhardt, L. A. Silks III, Z. Li, X. Yang, and B. I. Swanson. 2000. Characterization of Self-Assembled Monolayers for Biosensor Applications. *Langmuir* 16, 4 (2000), 1793–1800. doi:10.1021/la990018r

[14] G. E. Quintanilla-Villanueva, D. Luna-Moreno, Edgar Allan Blanco-Gámez, José Manuel Rodríguez-Delgado, J. Villarreal-Chiu, and M. Rodríguez-Delgado. 2021. A Novel Enzyme-Based SPR Strategy for Detection of the Antimicrobial Agent Chlorophene. *Biosensors* 11 (2021). doi:10.3390/bios11020043

[15] Debasis Samanta and Amitabha Sarkar. 2011. Immobilization of biomacromolecules on self-assembled monolayers: methods and sensor applications. *Chemical Society Reviews* 40 (2011), 2567–2592. doi:10.1039/c0cs00056f

[16] Oliver Seitz, Poornika G. Fernandes, Ruhai Tian, Nikhil Karnik, Huang-Chun Wen, Harvey Stiegler, Richard A. Chapman, Eric M. Vogel, and Yves J. Chabal. 2011. Control and stability of self-assembled monolayers under biosensing conditions. *Journal of Materials Chemistry* 21 (2011), 4384–4392. doi:10.1039/c1jm10132c

[17] Carlos Souza Filho, Antonio Marcus Lima, and Helmut Neff. 2008. Sistema de Aquisição e Processamento Portátil para Biosensores.. In *Anais do XVII Congresso Brasileiro de Automática.*

[18] Chaonan Sun, Xiaofang Liao, Pinxuan Huang, Guangzhi Shan, Xiao Ma, Lizhu Fu, Lidong Zhou, and Weijun Kong. 2020. A self-assembled electrochemical immunosensor for ultra-sensitive detection of ochratoxin A in medicinal and edible malt. *Food Chemistry* 315 (2020), 126289. doi:10.1016/j.foodchem.2020.126289

[19] C. Thirstrup, W. Zong, M. Borre, H. Neff, H.C. Pedersen, and G. Holzhueter. 2004. Diffractive optical coupling element for surface plasmon resonance sensors. *Sensors and Actuators B: Chemical* 100, 3 (2004), 298–308. doi:10.1016/j.snb.2004.01.010

[20] Jinru Zhou, Qinqin Qi, Chong Wang, Yifan Qian, Guangming Liu, Yanbo Wang, and L. Fu. 2019. Surface plasmon resonance (SPR) biosensors for food allergen detection in food matrices. *Biosensors & bioelectronics* 142 (2019), 111449. doi:10.1016/j.bios.2019.111449

[21] Tomáš Špringer, Markéta Bocková, Jiří Slabý, Foozieh Sohrabi, Magdalena Čapková, and Jiří Homola. 2025. Surface plasmon resonance biosensors and their medical applications. *Biosensors and Bioelectronics* 278 (2025), 117308. doi:10.1016/j.bios.2025.117308